

Electrochemical Detection of the Oligomerization of PB1-F2 Influenza A Virus Protein in Infected Cells

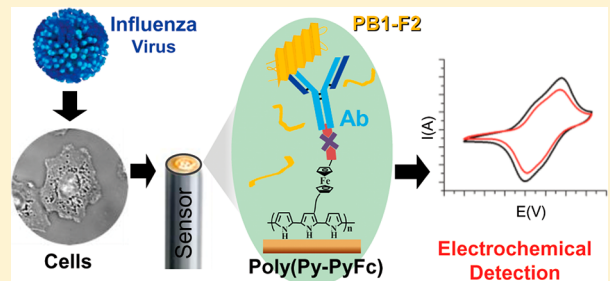
Anna Miodek,^{†,‡} Jasmina Vidic,^{*,‡} Helene Sauriat-Dorizon,[†] Charles-Adrien Richard,[‡] Ronan Le Goffic,[‡] Hafsa Korri-Youssoufi,^{*,†} and Christophe Chevalier^{*,‡}

[†]CNRS UMR-8182, Institut de Chimie Moléculaire et de Matériaux d'Orsay, Equipe de Chimie Bioorganique et Bioinorganique, Bâtiment 420, 91405 Orsay, France

^{*}INRA, Unité de Virologie et Immunologie Moléculaires, UR892, Domaine de Vilvert, F-78350 Centre de Jouy-en-Josas, France

Supporting Information

ABSTRACT: PB1-F2 is a nonstructural accessory protein of Influenza A virus described to enhance the mortality and the morbidity of the virus in a host-dependent manner. In this work, an electrochemical biosensor based on an immunodetection system was developed to follow the oligomerization of PB1-F2 during the viral cycle. The immunosensor was based on conductive polypyrrole modified with ferrocenyl groups as a redox marker for enhancing signal detection. Antibodies specific for monomeric or oligomeric PB1-F2 forms were immobilized on polypyrrole matrix via biotin/streptavidin layer. We demonstrated that this electrochemical biosensor sensitively detects PB1-F2 in both conformational forms. The linear range extends from 5 nM to 1.5 μ M and from 5 nM to 0.5 μ M for monomeric and oligomeric PB1-F2, respectively. The calculated limit of detection was 0.42 nM for monomeric PB1-F2 and 16 nM for oligomers. The biosensor platform allows the detection and quantification of PB1-F2 in lysates of infected cells during viral cycle. We show that at early stages of viral cycle, PB1-F2 is mainly monomeric but switched to amyloid-like structures at a later stage of infection. The quantification of two protein structural forms points out that PB1-F2 expression profiles and kinetics of oligomerization are cell-type-dependent.



Many neurodegenerative diseases, such as Alzheimer's or Parkinson's disease, are characterized by the intracellular or/and extracellular accumulation in tissues and organs of misfolded proteins in the form of fibrillar deposits. Proteins that undergo pathological structural rearrangements to form these fibers are either natively disordered proteins or proteins with destabilized native conformation. The amyloid nature of these assemblies is characterized by a common structural motif of a cross- β -sheet and the same cytotoxic activity associated with neurodegenerative diseases.^{1–3}

An increasing number of proteins unrelated to amyloid neurodegenerative pathologies are reported to aggregate into amyloid-type assemblies.⁴ They switch from a monomeric to an aggregated state that includes amyloid oligomers, prefibrillar assemblies, and mature fibers, sharing the same structural behavior as proteins involved in amyloid diseases.⁵ Recently, PB1-F2 protein of influenza A virus (IAV) was shown to form amyloid-like fibers in IAV-infected cells,⁶ but the kinetics of fibers formation, their intracellular localization, and their role in the viral cycle remain to be elucidated.

Every year, IAV, a member of the *Orthomyxoviridae* family,⁷ spreads on a worldwide scale and affects millions of people.⁸ PB1-F2 was discovered in 2001 and was initially described as a proapoptotic protein.⁹ Although expression of PB1-F2 is not necessary for developing an influenza infection, PB1-F2 was

reported to contribute to the immunopathological disorders developed during infection^{10,11} and to enhance secondary bacterial infections.¹²

PB1-F2 is a small protein of 87–90 amino acids which displays a strong polymorphism, in sequence and length.¹³ PB1-F2 is expressed in most human and avian IAV strains in its full-length version. PB1-F2 was described as a pro-apoptotic factor specifically inducing apoptosis in macrophages and monocytes and, thus, enhancing IAV virulence by compromising viral clearance.⁹ In contrast, PB1-F2 has no direct pro-apoptotic effect in epithelial cells.¹⁴ PB1-F2 has a short half-life and is expressed independently of the expression level of other influenza proteins.⁹

Although many studies focused on the immunoregulatory function of PB1-F2, very little structural information is available. Previous studies with recombinant PB1-F2 or synthetic peptides have shown that the conformation of PB1-F2 can switch according to the hydrophobicity of its environment.^{6,15} PB1-F2 has no secondary structure in aqueous solutions but adopts an α -helical structure within its positively charged C-terminal domain upon addition of trifluoroethanol.¹⁵

Received: May 14, 2014

Accepted: July 22, 2014

Published: July 22, 2014

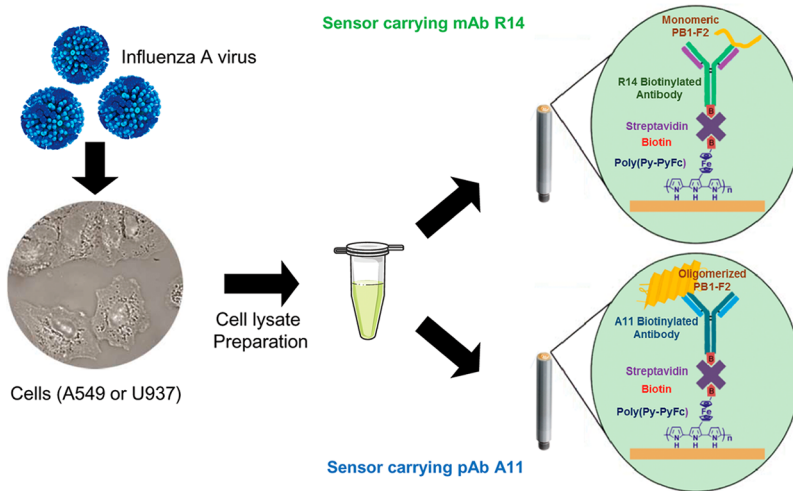


Figure 1. Overall scheme for the biosensor detection of both monomeric and oligomeric PB1-F2 in IAV-infected cells. The first sensor carried mAb R14 that specifically recognizes monomeric PB1-F2 in its random coil conformation, whereas the second carried pAb A11 that recognizes β -sheet epitope in amyloid oligomers.

Interestingly, PB1-F2 adopts a β -sheet conformation and oligomerizes to form amyloid-like fibers in a membrane-mimicking environment.⁶ The PB1-F2 amyloid structures were also detected in infected cells at the membrane vicinity. Recently, a study demonstrated the implication of PB1-F2 in the activation of the NLRP3 inflammasome in response to IAV infection and the induction of cytokine expression.¹⁶ This mechanism is triggered by the aggregated forms of PB1-F2 rather than by the soluble protein. This is in accordance with the well-known capability of amyloid fibers to specifically activate the NLRP3 inflammasome complex.¹⁷ Thus, the exacerbation of the host inflammatory response could be correlated with the ability of PB1-F2 to aggregate.¹⁸ To elucidate the putative role of fibrillated PB1-F2 in IAV infections and the kinetics of conversion of PB1-F2 from monomer to fiber, new analytical tools are needed.

Biosensors are an attractive solution for protein detection *in vivo* due to their simplicity, possible miniaturization, high sensitivity, and potential ability for real-time and on-site analysis. We have previously demonstrated that an electrochemical biosensor based on polypyrrole modified by redox probe allows detection of the monomeric form of PB1-F2 in the infected cell.¹⁹

In the present work, we develop an electrochemical biosensor platform carrying an oligomer-specific antibody recognizing the common β -sheet structural feature characterizing amyloid assemblies to allow a direct detection of amyloid oligomers formed by PB1-F2 in IAV-infected cells. Thus, combining monomer and oligomer detection, the biosensor platform (Figure 1) enabled us to follow the oligomerization of PB1-F2 from monomer to oligomer at different times of the viral cycle. In addition, we believe that our biosensor which recognizes a generic conformational epitope in amyloids offers a promising platform to study the kinetics of fibrillation of protein *ex vivo* as well as diseases caused by fibrillar assemblies of proteins.

MATERIALS AND METHODS

Production and Purification of PB1-F2 Protein. PB1-F2 protein of A/WSN/1933 (H1N1) influenza A virus (WSN) was expressed and purified as described previously.⁶ The

oligomerization of PB1-F2 was induced by incubating the recombinant protein with various concentration of SDS (0.0–2.0% w/v) in 5 mM sodium acetate buffer, pH 5, for 1 h at room temperature.

Cells Infection. The human alveolar epithelial cell line A549 and the human monocytic cell line U937 were purchased from the American Type Culture Collection. Cells were cultured and infected as previously described.²⁰ Cells were infected at a multiplicity of infection of 0.1 with WSN for 1 h at 37 °C, then incubated at 37 °C in complete medium until collection at 4, 6, 8, and 24 h postinfection. The total concentration of proteins in infected-cells lysate was evaluated using Bradford method.

Antibodies. The R14 rabbit hybridoma monoclonal antibody (mAb R14) directed against the full-length monomeric PB1-F2 was kindly provided from Dr J.F. Vautherot (INRA, France). Rabbit oligomer-specific polyclonal A11 antibody (pAb A11) was purchased from Invitrogen. Both antibodies were biotinylated using DSB-XTM Biotin Proteing Labeling Kit (Invitrogen), and labeled antibodies were purified using spin columns to discard any unreacted reagent.

Reagents. Pyrrole (Py), biotin hydrazide, and streptavidin were purchased from Sigma-Aldrich. Py was distilled under argon before use. The modified pyrrole monomer, 1-(phtalimidylbutanoate)-1'-(*N*-(3-butylpyrrole)butanamide) ferrocene (Py-Fc-NHP), was synthesized according to the procedure described previously.¹⁹ Analyses were performed in phosphate buffer saline containing 10 mM Na₂HPO₄, 1.8 mM KH₂PO₄, 2.7 mM KCl, and 137 mM NaCl, pH 7.4, (PBS) or in 5 mM sodium acetate buffer, pH 5.0. Buffers were filtered through 0.2 μ m membranes before use.

Electrochemical Measurements. Electrochemical measurements were performed using a potentiostat Autolab PGSTAT 12 controlled by Autolab GPES software. The detection of PB1-F2 in infected cells was performed using portable potentiostat Autolab PGSTAT 101 controlled by Nova software (Metrohm). The electrochemical three-electrode cell was equipped with a gold disc as a working electrode with a surface of 0.02 cm², the platinum wire served as an auxiliary electrode and the Ag/AgCl electrode as a reference electrode. Cyclic Voltammetry (CV) was performed

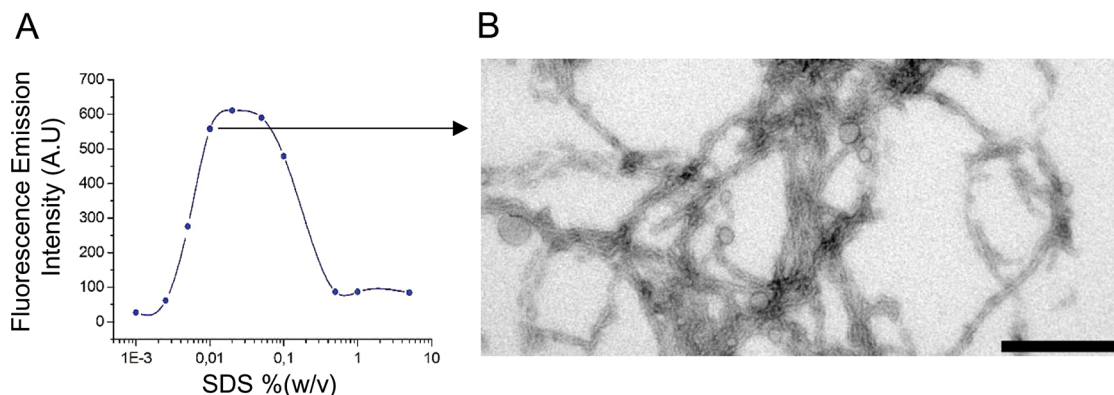


Figure 2. Detection of amyloid-like structures formed by recombinant PB1-F2 in vitro. (A) Enhancement of ThT fluorescent emission after its binding to amyloid-like particles formed by 10 μ M PB1-F2 in the presence of various concentrations of SDS in 5 mM sodium acetate buffer, pH 5. Note that amyloids assembled only within a narrow range of SDS concentrations. (B) Transmission electron microscopy observation of the PB1-F2 aggregates formed in the presence of 0.01% w/v SDS. Bar = 200 nm.

in the range of potential from -0.4 to 0.6 V with scan rate of 100 mVs $^{-1}$. The CV measurement was performed in PBS buffer for biosensor construction and in sodium acetate buffer during PB1-F2 detection.

AFM Measurements. A commercial dimension 3100 AFM (Vecco Instruments) was used for topographical characterization of the PB1-F2 captured on the sensor surface. All measurements were performed at the tapping mode for a ($1\text{ }\mu\text{m} \times 1\text{ }\mu\text{m}$) surface using rectangular silicon AFM tip.

Electron Microscopy. Electron microscopy was applied to visualize the amyloid-like structures of PB1-F2. PB1-F2 was incubated in sodium acetate buffer with 0.01% w/v SDS at room temperature for 30 min. A $10\text{ }\mu\text{L}$ sample was placed on Formvar-coated copper grids (Agar Scientific). Then, the samples were negatively stained with 2% uranyl acetate (Sigma) for 1 min. The grids were air-dried before observation under a Zeiss EM902 TEM operated at 80 kV (Carl Zeiss).

Thioflavin T Fluorescence Measurements. Thioflavin T (ThT) staining was performed to characterize the amyloid nature of recombinant PB1-F2 structures. ThT fluorescence was measured using a Jasco FR-6200 spectrophotofluorometer in 1 mm optical path-length quartz cuvettes at 20°C . The assay was performed by adding freshly prepared ThT solution to PB1-F2 samples in equimolar ratio in sodium acetate buffer, pH 5. Excitation was performed at 432 nm.

Electropolymerization. Electropolymerization was performed to functionalize the surface of the gold electrode with biotin groups. During electropolymerization, working and auxiliary electrodes were separated in sample chamber placed in a cell stand containing the Ag/AgCl reference electrode. The copolymer film was grown on the gold surface in a 0.5 M acetonitrile solution containing 0.5 M LiClO₄ and a mixture of Py and Py-Fc-NHP monomers at a concentration ratio of 8:2 mM.²¹ The electropolymerization was performed by cycling the potential from -0.4 to 0.95 V with a scan rate of 100 mVs $^{-1}$. The reaction was stopped when the reduction current intensity of ferrocene reached $30\text{ }\mu\text{A}$. The modified gold electrode was washed with acetonitrile and double-distilled water to eliminate nonpolymerized molecules.

Construction of Biosensor. Each step of the biosensor construction was performed by placing $40\text{ }\mu\text{L}$ of analyte in 10 mM PBS buffer solution pH 7.4 on the surface of the working electrode at room temperature. The bilayer was formed by successive reaction with $40\text{ }\mu\text{L}$ of biotin hydrazide (2 mg·

mL $^{-1}$), streptavidin ($100\text{ }\mu\text{L}\cdot\text{mL}^{-1}$), and biotinylated mAb R14 or pAb A11 ($8\text{ }\mu\text{g}\cdot\text{mL}^{-1}$) during 45 min at room temperature. After each step, the modified surface was washed with water and PBS buffer to eliminate the residues nonbonded on the surface after each step of the biosensor construction. Before protein detection, biosensor was stabilized in 5 mM sodium acetate buffer pH 5 at 4°C overnight. After this step, the electrochemical response of the biosensor remains stable. The stability of electrochemical response of biosensors was studied during 2 weeks, and no significant variation was observed.

Detection of PB1-F2 by Biosensors. To detect PB1-F2, the sensor surface was incubated with the protein solution for 40 min at room temperature before measuring. After each measurement, the electrode was washed with sodium acetate buffer to eliminate nonlinked proteins. Prior to detect oligomeric PB1-F2, the recombinant protein was incubated with different concentration of SDS (0.0–2.0% w/v) in 5 mM sodium acetate buffer, pH 5, for 1 h.

RESULTS AND DISCUSSION

Oligomerization of Recombinant PB1-F2 in Vitro. PB1-F2 was previously demonstrated to adopt β -sheet conformation and to oligomerize to amyloid-like fibers in hydrophobic and membrane environment.⁶ In order to mimic the lipid environment, a range of concentration of an anionic detergent, SDS (0.0–2.0%) was used to induce PB1-F2 oligomerization in vitro (Figure 2A). Samples were stained with ThT to reveal the formation of amyloid structures. Indeed, ThT specifically binds to β -sheet motif characterizing amyloid assemblies which results in enhancement of ThT fluorescence emission. In sodium acetate buffer, PB1-F2 is nonstructured and did not bind ThT. Within a sharp range of SDS concentrations (0.005–0.1%), PB1-F2 enhanced ThT fluorescence by a factor of more than 200, strongly suggesting the formation of amyloid-like structures. The maximum of ThT fluorescence intensity was reached between 0.01 and 0.05% w/v of SDS (Figure 2A). No significant ThT staining was observed in solutions containing SDS concentrations equal or superior to its critical micellar concentration (0.23% w/v.). Electron transmission microscopy revealed fibrillar aggregates of different sizes in the buffer solution containing 0.01% w/v of SDS (Figure 2B). The fibrillar and granular structures observed are similar to the amyloid assemblies found in various neurodegenerative diseases.

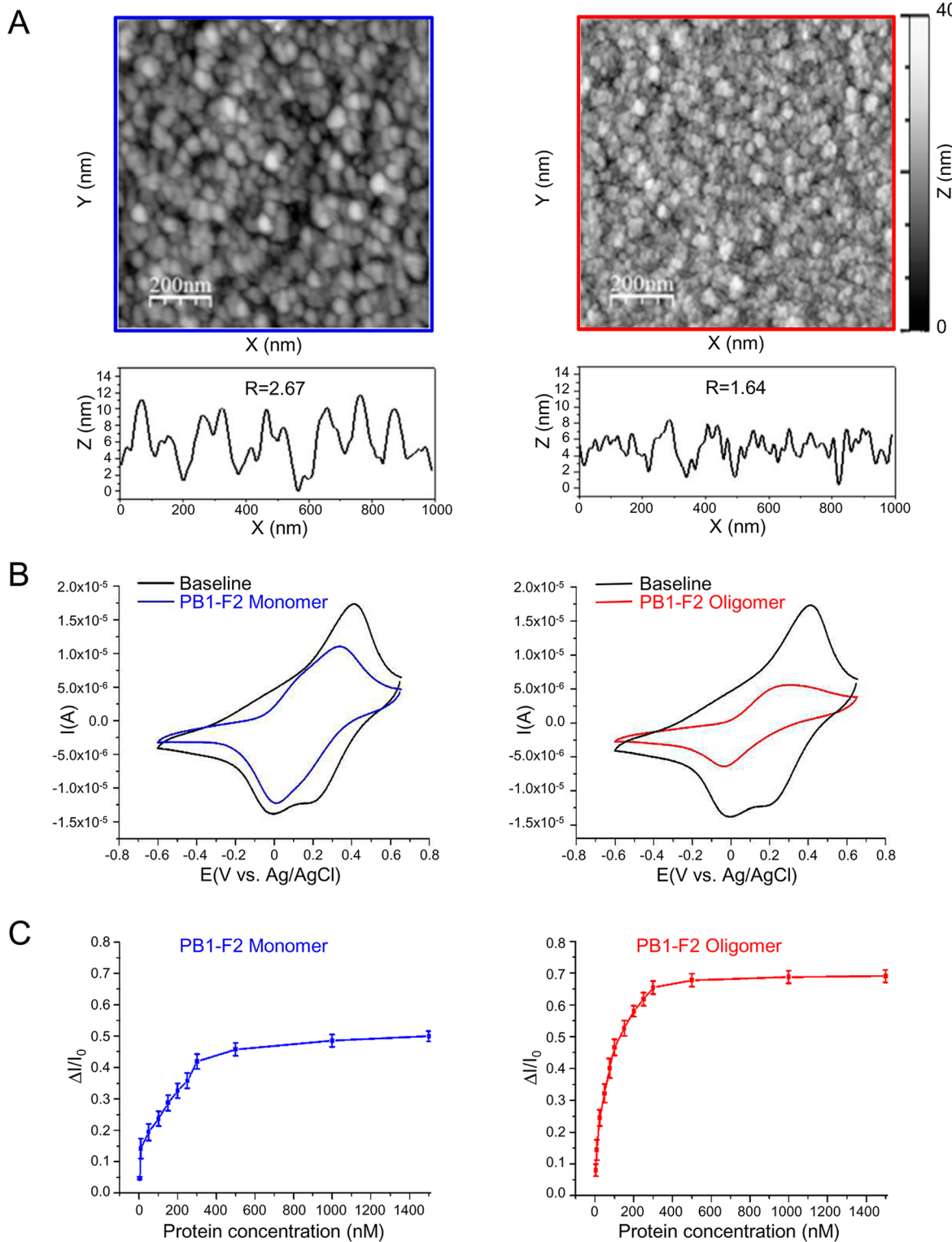


Figure 3. Biosensors detections of PB1-F2 in monomeric and oligomeric forms. (A) Topographic AFM images ($1 \mu\text{m} \times 1 \mu\text{m}$) of a gold surface modified with copolymer film carrying mAb R14 antibody (left panel) or pAb A11 (right panel) after binding monomeric PB1-F2 or oligomerized PB1-F2 respectively. (B) CVs recorded before and after addition of 500 nM of monomeric PB1-F2 onto the sensor carrying mAb R14 (left panel) or oligomerized PB1-F2 onto the sensor carrying pAb A11 (right panel). Baselines were recorded by immersion of the sensor in sodium acetate buffer alone. (C) Calibration curves showing the variations of oxidative ferrocene currents as a function of the different concentrations of monomeric (left panel) or oligomeric (right panel) PB1-F2 probed by the corresponding sensors. Data points are the mean values \pm SD obtained in three independent experiments.

Biosensing Recombinant PB1-F2 in Monomeric and Oligomeric States. Two antibodies were used to detect PB1-F2: mAb R14, which specifically recognizes the monomeric

random coiled form of PB1-F2,^{6,20} and pAb A11, a conformational antibody raised against a generic conformational β -sheet epitope present in amyloid oligomers.^{1,22} The elaboration of an

electrochemical biosensor based on mAb R14 to detect monomeric PB1-F2 protein in biological samples was described previously.¹⁹ Here, to detect separately monomeric and oligomeric PB1-F2, the two antibodies mAb R14 and pAb A11 were separately anchored onto the copolymer poly(Py-PyFcNHP) layer via the biotin/streptavidin pair (Figure 1). The ferrocenyl group linked covalently to polypyrrole exhibits an intense and sensitive electrochemical signal at 0.4 V vs Ag/AgCl allowing electrochemical measuring the antibody/protein interaction. The ferrocene signal amplitude decreases when the antibody/PB1-F2 complex is formed, because the molecular assemblies formed on the electrode hinder the electron transfer process and the ion penetration to the sensor surface.¹⁹

Figure 3A shows AFM images of the functionalized electrochemical biosensor surfaces bearing either mAb R14/monomeric PB1-F2 (left panel) or bearing pAb A11/oligomerized PB1-F2 (right panel) complexes. The topology of the surfaces was different because the biosensors recognize PB1-F2 in forms of different sizes. The capture of monomeric PB1-F2 with the mAb R14 led to regular and well organized topology consisting of particles of about 5 to 10 nm. This average size measured is in accordance with the mean hydrodynamic radius of monomeric PB1-F2 previously reported.⁶ The calculated roughness factor was 2.67. In contrast, the biosensor capturing PB1-F2 oligomers exhibited a dense and homogeneous surface with a lower roughness factor of 1.64. This lower factor corresponds to the capture of PB1-F2 particles of larger sizes than the monomeric protein.

The CV curves of the biosensors detecting monomeric or oligomeric PB1-F2 forms are presented in Figure 3B. A decrease in both reductive and oxidative ferrocene peaks was observed after the detection of monomeric PB1-F2 or oligomerized PB1-F2 by the biosensor carrying mAb R14 (left panel) or pAb A11 (right panel), respectively. The signal decreases originated from the lower charge transfer due to the blocking effect of the antibody–antigen complex formation on the surface. As illustrated in Figure 3B, 500 nM of oligomeric PB1-F2 (monomer unit equivalents) led to a larger variation in current density compared to the signal variation obtained with the same concentration of monomeric PB1-F2. Observed difference in current variation of redox ferrocene signal was expected considering the differences in sizes between monomeric and oligomeric protein forms. Binding of large protein assemblies obstructs the charge transfer and ions diffusion in the immobilized layer on the electrode more importantly. For both biosensors, variations of electrochemical responses depended on the concentration of PB1-F2 deposited on the biosensor surfaces. To draw calibration curves, measurements were realized with the range of recombinant PB1-F2 protein concentrations from 5 nM to 5 μM in the sodium acetate buffer solution without SDS, or containing 0.05% w/v SDS for monomer and oligomer detection, respectively. CVs were recorded after successive incubation of the modified electrodes with increasing concentrations of PB1-F2. The calibration curves (Figure 3C) were plotted as a variation of anodic current of ferrocenyl group at 0.4 V versus Ag/AgCl, versus the concentration of PB1-F2 deposited on the two biosensors. For monomeric PB1-F2, a dynamic range of detection was obtained for concentrations ranging from 5 nM to 1.5 μM. The saturation signal of biosensor was observed at 1.5 μM PB1-F2. A detection limit of 0.42 nM was calculated according to the signal-to-noise ratio of 3 independent measurements, taking into account the standard deviation of

0.012 and the sensitivity deduced from the slope of the linear curve obtained for low concentrations of PB1-F2. The selectivity of mAb R14 was confirmed with various proteins of similar net charge and molecular weight (Shadoo, A-β, and N-terminal part of prion protein).¹⁹ For oligomeric PB1-F2, a dynamic range of detection from 5 nM to 500 nM was obtained, showing a linear part from 10 to 100 nM with a calculated detection limit of 16 nM. Measurements were highly reproducible with only 1–3% of relative standard deviation for three independent measurements obtained with freshly prepared biosensors.

Conformational Specificity of Biosensors for PB1-F2 Detection.

The cross reactivity of immobilized antibodies was checked to assess biosensors specificity. Recombinant PB1-F2 was incubated in sodium acetate buffer solutions containing various concentrations of SDS (0–0.2% w/v). Note that PB1-F2 oligomerizes in SDS solution ranging from 0.005 to 0.1% w/v (Figure 2A). Indeed, biosensor carrying mAb R14 showed maximal signal for PB1-F2 monomer detection in solutions with SDS concentrations inferior to 0.01 or superior to 0.2% w/v SDS (Figure 4A, i.e., conditions not favorable for oligomer

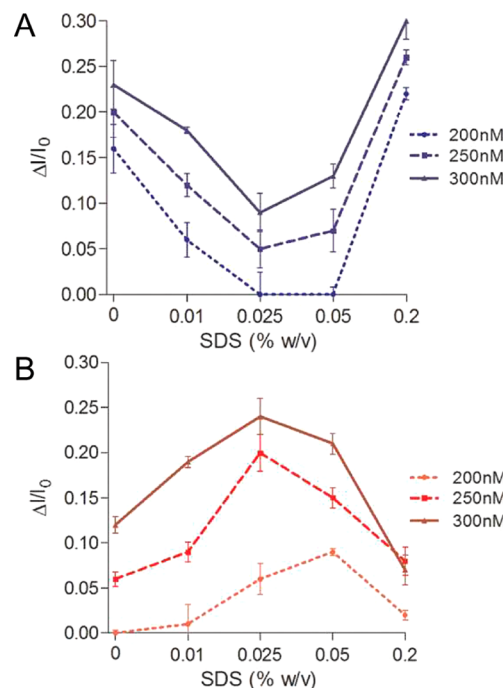


Figure 4. Relative current intensities corresponding to the detection of three different concentrations of recombinant PB1-F2 in monomeric (A) and oligomeric (B) forms as a function of SDS concentration. A threshold subtraction was applied to the presented curves. The content of PB1-F2 solutions containing various proportions of monomeric/oligomeric forms depending on the SDS concentration was probed with biosensors carrying either mAb R14 (blue curves) or pAb A11 (red curves).

formation). In contrast, the signal obtained with biosensor carrying pAb A11 reached a maximum in a sharp range of SDS concentrations from 0.025 to 0.05% w/v (Figure 4B, i.e., concentrations of SDS that induce pronounced oligomerization of PB1-F2). Our results confirm the conformational specificity of both biosensors for detection of two different forms of PB1-F2. The result obtained suggest that oligomerization induces

A549

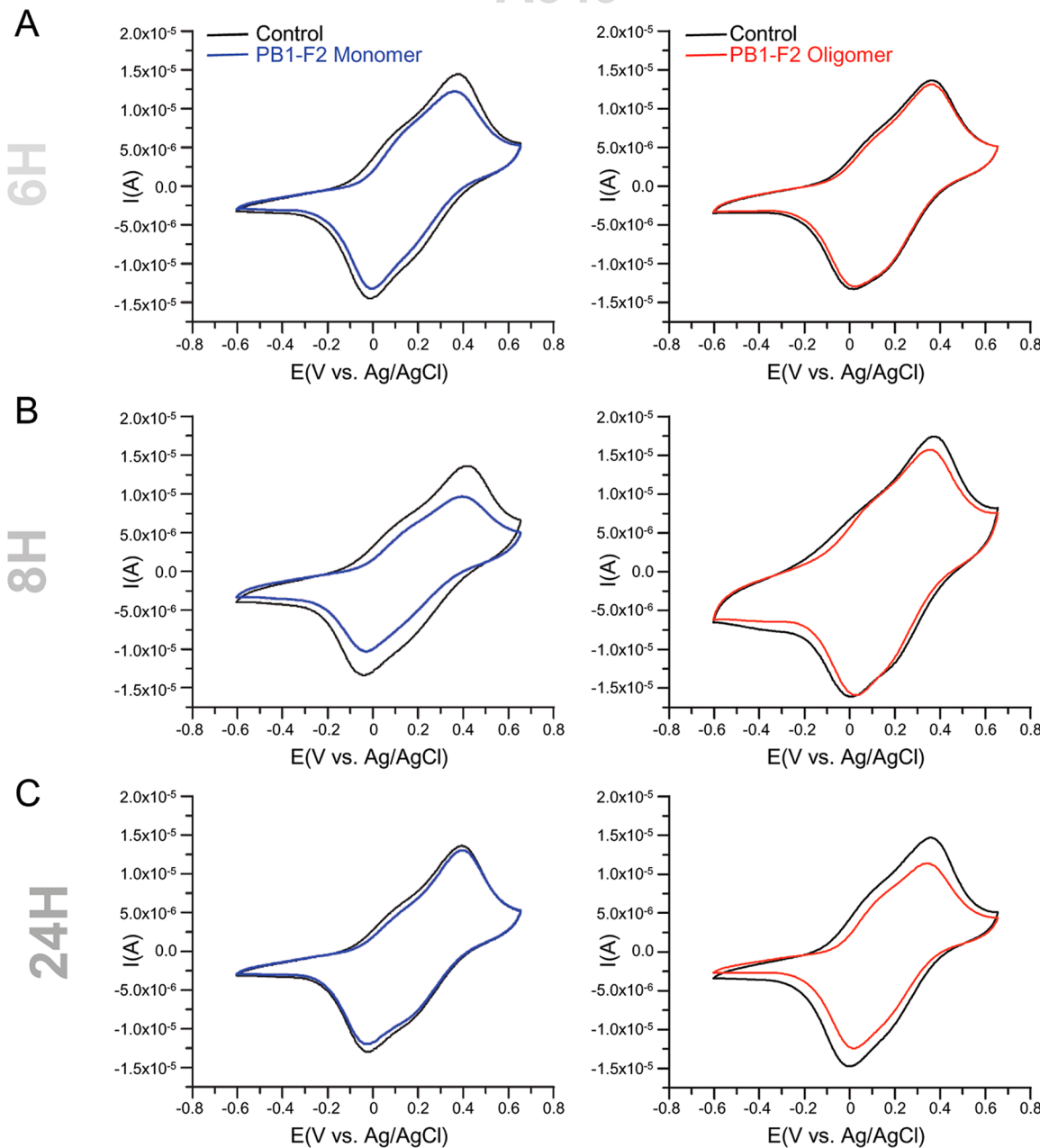


Figure 5. CV curves obtained before (black) and after detection of monomeric (blue) and oligomeric (red) PB1-F2 in IAV-infected epithelial human A549 cells. Infected cells were collected at (A) 6 h, (B) 8 h, and (C) 24 h post infection and corresponding cells lysates were prepared and subjected to electrochemical measurements.

conformational changes of PB1-F2 that prevent accessibility of the epitope region of PB1-F2 which is recognized by mAb R14.

Detection in Infected Cells. We next applied the developed biosensors to detect monomeric and oligomeric PB1-F2 in IAV-infected cells at various times of the virus cycle. Human epithelial cells A549 and human monocyte U937 cells were used because these cell types are relevant in vitro cellular models of influenza virus targets. Cells were infected with A/WSN/1933 (H1N1) virus and collected at various times postinfection. Lysates of infected cells adjusted to 0.1 mg/mL of total proteins were loaded onto biosensor surface without any additional labeling.

Figure 5 shows CVs recorded after the immersion of two biosensors into the cell lysates of A549. A decrease of ferrocenyl group redox currents was observed with the biosensor carrying mAb R14 emerged into lysates of infected cells at 4, 6, and 8 h postinfection. The reduction of the current reflects the binding of PB1-F2 from the lysates to the immobilized antibody. In contrast, there was no significant current variation upon mAb R14 biosensor incubation with cell lysates obtained 24 h postinfection (Figure 5C). Similarly, monomeric PB1-F2 was detected in cell lysates of infected U937 only at early stage of infection (Figure S-1). The concentration of monomeric PB1-F2 in infected cells was evaluated by reporting the current variation to the calibration

curve obtained with recombinant PB1-F2, presented in Figure 3C (left panel). The quantity of monomeric PB1-F2 at various times postinfection was calculated relative to 1 mg of total proteins in IAV-infected cells and presented as histograms in Figure 6. Intriguingly, the maximum signal variation obtained with biosensor carrying mAb R14 was reached at 8 h postinfection in A549 lysate against 6 h postinfection in U937 lysate. This feature suggests a different expression pattern of monomeric PB1-F2 in the two cell types.

The biosensor based on pAb A11 incubated with cell lysates showed no significant current variation at early stages postinfection (Figure 5A). The maximum variation was observed for 24 h postinfection, as illustrated for A549 in Figure 5C and for U937 in Figure S-1. On the basis of the calibration curve in Figure 3C (right panel), PB1-F2 oligomer concentration was quantified in both cell types at various times post infection and expressed relative to 1 mg/mL of total cell proteins in Figure 6. However, PB1-F2 oligomers were detected

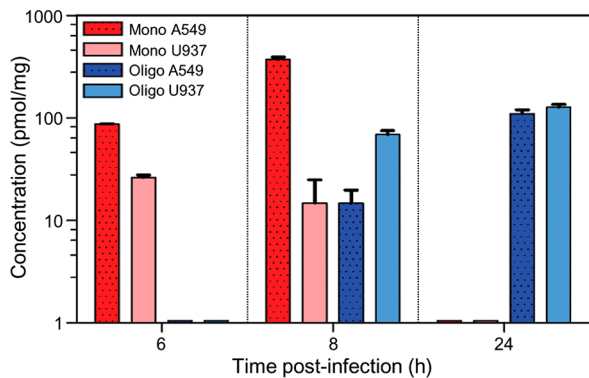


Figure 6. Histograms representing the quantification of detected monomeric (blue) and oligomeric (red) PB1-F2 in IAV-infected A549 or U937 cell lysates using the electrochemical immunosensors. The quantification was done using the calibration curves from Figure 3C and expressed relative to 1 mg of total proteins in lysates.

starting from 8 h postinfection in both cell-types. It appears that formation of PB1-F2 oligomers in U937 monocytes is accompanied by the complete disappearance of monomeric PB1-F2, suggesting a total switch from the monomeric to oligomeric state. In contrast, monomeric PB1-F2 is still detectable at 8 h postinfection in A549 epithelial cells, suggesting only partial oligomerization of PB1-F2 at that time. Finally, at 24 h postinfection, when oligomers reached maximum concentration, no monomeric PB1-F2 was detectable in both cell-types.

To verify the sensitivity and selectivity of biosensors for detection of PB1-F2, control experiments were performed using noninfected cells (NI) (Figure S-2) and cells infected by the PB1-F2 knockout mutant virus (Δ F2) (Figure S-3). Previous investigations have shown that there is no significant difference in progeny virus titers between wild type and Δ F2 upon infection of various cell lines and tissues.¹¹ The CVs obtained before and after incubation of biosensors in lysates of NI- and Δ F2-infected cells show no significant variation of the current. Thus, the control experiments confirm the high specificity of biosensors to PB1-F2 in infected cells.

PB1-F2 is an intrinsically disordered protein capable to change its conformation depending on its environment.⁶ Disordered proteins are implicated in various cell regulatory functions that imply their direct interaction with some cellular

interactors.²³ Consequently, the conformation and function of nonstructured proteins depend on their specific cellular partners and may be cell-type-dependent. Moreover, it was shown that conformational conversion of proteins involved in neurodegenerative diseases can be modulated by various cellular components such as nucleic acids, lipids, or chaperones.^{24,25} Up to now, PB1-F2 was described to interact with several protein as VDAC-1, ANT-3,¹⁴ or MAVS.²⁶ However, a complete screening of its potential cellular interactors has not yet been performed. Interestingly, different PB1-F2 impacts were reported depending of the cell-type: PB1-F2 induces apoptosis in U937 cells while it promotes inflammation in A549 cells.¹¹ We can hypothesize that the function of PB1-F2 depends on the conformational state that the protein adopts in a given host cell type.

Conventional techniques applied in previous works, such as Western blot^{6,9,11} and SPR,^{11,20} are not convenient for studying aggregation/oligomerization of proteins in viral context because they are limited by the accessibility of the specific protein epitope. Previous studies reported a transient expression of PB1-F2 during the early steps of the virus cycle and a propensity for degradation because the protein is barely detectable at 10 h post infection or later.^{9,11} Our results show for the first time that PB1-F2 after being expressed as monomer at early stages of infection, accumulates as oligomers within the infected cells at later stages of infection. The cellular factors triggering this process remain to be identified to get a better understanding of the structural behavior of PB1-F2 in the different cell types.

Up to now, most electrochemical sensing systems developed to detect aggregated proteins are based on indirect measurements requiring elaborate protocols.²⁷ This typically involved an oxidation of intrinsically electroactive amino acid residues accessible only within the natively folded protein or an electrochemical detection of hydrogen production coming from catalytic reaction of aggregated protein.²⁷ Also, an electroactive mediator intercalating β -sheet motif can be monitored to allow indirect detection of amyloid structures. Only impedance spectroscopy with surface-immobilized $\text{A}\beta$ -amyloid fibers has been performed to follow the protein interaction with potential drugs in a direct way.²⁸ All these methods have been performed with purified protein while no measurement was described *in vivo* or *ex vivo*.

Herein we demonstrate that electrochemical biosensors can be applied to detect conformational conversion from monomeric to amyloid-like structure of PB1-F2 during the viral cycle of influenza virus. Our results obtained with immunosensors open the way for developing electrochemical technology to detect viral proteins and their aggregation within infected cells or other biological samples.

CONCLUSIONS

PB1-F2 was reported to contribute to the pathology of IAV-viruses via various immunological deregulations in infected cells. Although the PB1-F2 mechanism of action remains to be elucidated it seems to be virus-strain- and cell-type-dependent. We have developed sensitive electrochemical sensors based on polypyrrole and ferrocenyl group as a redox marker for detection and quantification of monomeric and oligomeric PB1-F2 in IAV-infected cells. Recombinant PB1-F2 was used to demonstrate the specificity and selectivity of the sensors for detection of the protein in both conformational forms. Developed sensors were successfully applied to follow PB1-

F2 expression patterns during the viral cycle in two different cell types. We observed that monomeric PB1-F2 protein accumulates within the infected cells at early stages of viral cycle and is barely detectable after 8 h postinfection. Even if we cannot rule out that PB1-F2 is partially degraded at later stage of infection as previously proposed in the literature, we showed here for the first time that absence of monomeric PB1-F2 is correlated with the formation of PB1-F2 oligomers. Our results suggest that electrochemical immunosensor technology may be applied to detect other proteins that form amyloid oligomers and thus may represent new diagnostic tools for amyloid-related diseases.

■ ASSOCIATED CONTENT

Supporting Information

Detection of monomeric and oligomeric PB1-F2 in IAV-infected human monocyte U937 cells, DF2-infected human epithelial A549 cells, and DF2-infected human monocyte U937 cells. This material is available free of charge via the Internet at <http://pubs.acs.org>.

■ AUTHOR INFORMATION

Corresponding Authors

*E-mail: jasmina.vidic@jouy.inra.fr. Fax: +33 1 34652621. Tel.: +33 1 34652623.

*E-mail: hafsa.korri-youssoufi@u-psud.fr. Fax: +33 1 69157281. Tel.: +33 1 69157440.

*E-mail: christophe.chevalier@jouy.inra.fr. Fax: +33 1 34652621. Tel.: +33 1 34 65 2605.

Notes

The authors declare no competing financial interest.

■ ACKNOWLEDGMENTS

We gratefully thank Sophie Chat and Christine Longin (INRA Jouy-en-Josas) for electronic microscopy observations, Mohammed Moudjou (INRA Jouy-en-Josas) for protein purification, Jean-François Vautherot (INRA Tours) for providing the monoclonal antibody R14, and Edith Pajot-Augy (INRA Jouy-en-Josas) for critical reading of the manuscript. This work was supported by France Government CNRS and INRA institutions, and we also acknowledge the Ministry of Higher Education and Research for the Graduate Research Fellowship (to A.M.).

■ REFERENCES

- (1) Kayed, R.; Head, E.; Thompson, J. L.; McIntire, T. M.; Milton, S. C.; Cotman, C. W.; Glabe, C. G. *Science* **2003**, *300*, 486–489.
- (2) Lambert, M. P.; Barlow, A. K.; Chromy, B. A.; Edwards, C.; Freed, R.; Liosatos, M.; Morgan, T. E.; Rozovsky, I.; Trommer, B.; Viola, K. L.; Wals, P.; Zhang, C.; Finch, C. E.; Krafft, G. A.; Klein, W. L. *Proc. Natl. Acad. Sci. U.S.A.* **1998**, *95*, 6448–6453.
- (3) Bucciantini, M.; Giannoni, E.; Chiti, F.; Baroni, F.; Formigli, L.; Zurdo, J.; Taddei, N.; Ramponi, G.; Dobson, C. M.; Stefani, M. *Nature* **2002**, *416*, 507–511.
- (4) Stefani, M. *Prog. Neurobiol.* **2012**, *99*, 226–245.
- (5) Stefani, M.; Dobson, C. M. *J. Mol. Med.* **2003**, *81*, 678–699.
- (6) Chevalier, C.; Al Bazzal, A.; Vidic, J.; Fevrier, V.; Bourdieu, C.; Bouguyon, E.; Le Goffic, R.; Vautherot, J. F.; Bernard, J.; Moudjou, M.; Noinville, S.; Chich, J. F.; Da Costa, B.; Rezaei, H.; Delmas, B. *J. Biol. Chem.* **2010**, *285*, 13233–13243.
- (7) *Influenza Virology: Current Topics*; Kawaoka, Y., Ed.; Caister Academic Press: Wymondham, U.K., 2006.
- (8) WHO. Global Influenza Surveillance and Response System (GISRS). Website: http://www.who.int/influenza/gisrs_laboratory/en/ (accessed 2014).
- (9) Chen, W.; Calvo, P. A.; Malide, D.; Gibbs, J.; Schubert, U.; Bacik, I.; Basta, S.; O'Neill, R.; Schickli, J.; Palese, P.; Henklein, P.; Bennink, J. R.; Yewdell, J. W. *Nat. Med.* **2001**, *7*, 1306–1312.
- (10) Le Goffic, R.; Leymarie, O.; Chevalier, C.; Rebours, E.; Da Costa, B.; Vidic, J.; Descamps, D.; Sallenave, J. M.; Rauch, M.; Samson, M.; Delmas, B. *PLoS Pathog.* **2011**, *7*, e1002202.
- (11) Le Goffic, R.; Bouguyon, E.; Chevalier, C.; Vidic, J.; Da Costa, B.; Leymarie, O.; Bourdieu, C.; Decamps, L.; Dhorne-Pollet, S.; Delmas, B. *J. Immunol* **2010**, *185*, 4812–4823.
- (12) McAuley, J. L.; Hornung, F.; Boyd, K. L.; Smith, A. M.; McKeon, R.; Bennink, J.; Yewdell, J. W.; McCullers, J. A. *Cell Host Microbe* **2007**, *2*, 240–249.
- (13) Zell, R.; Krumbholz, A.; Eitner, A.; Krieg, R.; Halbhuber, K. J.; Wutzler, P. *J. Gen. Virol.* **2007**, *88*, 536–546.
- (14) Zamarin, D.; Garcia-Sastre, A.; Xiao, X.; Wang, R.; Palese, P. *PLoS Pathog.* **2005**, *1*, e4.
- (15) Bruns, K.; Studtrucker, N.; Sharma, A.; Fossen, T.; Mitzner, D.; Eissmann, A.; Tessmer, U.; Roder, R.; Henklein, P.; Wray, V.; Schubert, U. *J. Biol. Chem.* **2007**, *282*, 353–363.
- (16) McAuley, J. L.; Tate, M. D.; MacKenzie-Kludas, C. J.; Pinar, A.; Zeng, W.; Stutz, A.; Latz, E.; Brown, L. E.; Mansell, A. *PLoS Pathog.* **2013**, *9*, e1003392.
- (17) Masters, S. L.; Dunne, A.; Subramanian, S. L.; Hull, R. L.; Tannahill, G. M.; Sharp, F. A.; Becker, C.; Franchi, L.; Yoshihara, E.; Chen, Z.; Mullooly, N.; Mielke, L. A.; Harris, J.; Coll, R. C.; Mills, K. H.; Mok, K. H.; Newsholme, P.; Nunez, G.; Yodoi, J.; Kahn, S. E.; Lavelle, E. C.; O'Neill, L. A. *Nat. Immunol.* **2010**, *11*, 897–904.
- (18) Leymarie, O.; Jouvion, G.; Herve, P. L.; Chevalier, C.; Lorin, V.; Lecardonnel, J.; Da Costa, B.; Delmas, B.; Escriou, N.; Le Goffic, R. *PLoS One* **2013**, *8*, e57894.
- (19) Miodek, A.; Sauriat-Dorizon, H.; Chevalier, C.; Delmas, B.; Vidic, J.; Korri-Youssoufi, H. *Biosens. Bioelectron.* **2014**, *59C*, 6–13.
- (20) Vidic, J.; Chevalier, C.; Le Goffic, R.; Miodek, A.; Bourdieu, C.; Richard, C.-a.; Moudjou, M.; Delmas, B. *J. Anal. Bioanal. Tech.* **2013**, DOI: 10.4172/2155-9872.S4177-4006.
- (21) Le, H. Q.; Sauriat-Dorizon, H.; Korri-Youssoufi, H. *Anal. Chim. Acta* **2010**, *674*, 1–8.
- (22) Vidic, J.; Le Goffic, R.; Miodek, A.; Bourdieu, C.; Richard, C.-a.; Moudjou, M.; Delmas, B.; Chevalier, C. *J. Anal. Bioanal. Tech.* **2013**, DOI: 10.4172/2155-9872.1000169.
- (23) Wright, P. E.; Dyson, H. J. *J. Mol. Biol.* **1999**, *293*, 321–331.
- (24) Steunou, S.; Chich, J. F.; Rezaei, H.; Vidic, J. *Biosens. Bioelectron.* **2010**, *26*, 1399–1406.
- (25) Li, Q.; Chevalier, C.; Henry, C.; Richard, C. A.; Moudjou, M.; Vidic, J. *Biochem. Biophys. Res. Commun.* **2013**, *438*, 519–525.
- (26) Varga, Z. T.; Grant, A.; Manicassamy, B.; Palese, P. *J. Virol.* **2012**, *86*, 8359–8366.
- (27) Veloso, A.; Kerman, K. *Anal. Bioanal. Chem.* **2013**, *405*, 5725–5741.
- (28) Szymanska, I.; Radecka, H.; Radecki, J.; Kalisz, R. *Biosens. Bioelectron.* **2007**, *22*, 1955–1960.